Charge Density Analysis of Atomic Functions, Atomic Excitation, and Single Ionization

Bernard J. Ransil*[1a] and John J. Sinai[1b]

Contribution from the Harvard Medical Unit, Boston City Hospital, Boston, Massachusetts 02118, and the Department of Physics, University of Louisville, Louisville, Kentucky 40208. *Received March 28, 1972*

Abstract: Charge density analysis of molecule formation implies an explicit understanding of free atom charge density distributions. To this end, certain quantifiable electron charge density properties—the electron density at the nucleus, ρ_N, integer electron populations, $P(e)$, and their associated radii, $r(e)$—are defined and tabulated for first and second row neutral atoms, ions, and selected excited states. These properties may be used to analyze a variety of structural problems, both atomic and molecular. Specific problems discussed here are: the charge density redistributions associated with atomic ionization and excitation, the "quality" of atomic wave functions, and the appropriate atomic ground state charge density distribution for determining molecular charge density difference distributions. The analysis reveals internal inconsistencies in the atomic basis sets used and leads to the suggestion that maximization of the nuclear electron density, or agreement with its experimental equivalent Q_0[c] where available, be considered additional criteria for calculating accurate wave functions. Atomic p-electron excitation results in a charge buildup at and near the nucleus, with a corresponding charge depletion elsewhere, in such a way that certain integer electron "core populations" remain unchanged. Single positive ion formation for B → F results in charge buildup at and near the nucleus and a charge depletion elsewhere. The reverse is true for single negative ion formation. The existence of a "density discontinuity" between the series Li → Be and B → F that parallels the "bond discontinuity" reported for dipole moments is demonstrated.

The relationship of localized electron charge to chemical binding has been the subject of many studies beginning with the postulation of the Lewis structures and Mulliken's population analyses. A recent group of papers[2] presented total charge density and density difference contour maps for a series of first and second row diatomic molecules and discussed bonding in terms of a forces-on-nuclei model introduced by Berlin.[3a] The resultant explanation of bonding, considering each molecular orbital in turn, is complex, even for diatomic molecules. Consequently, its application to larger molecules, especially those of biological interest, seems remote.

In another paper, hereafter designated as RS 1967,[3b] the present authors concentrated upon certain regions of space defined by the redistribution of charge in the process of molecule formation. The scope of that study and the conclusions reached at that time (1962–1966) were restricted by the lack of accurate, internally consistent sets of wave functions for a sufficiently large representative group of atoms and molecules.

Since then this deficiency has been corrected somewhat and it now seems appropriate to attempt further development. One conclusion reached at that time was that base line information about free atom charge densities would be a necessary prerequisite to any further study of charge redistribution in molecule formation. To that end, in this study, we examine free atom charge density distributions and define certain numerical quantities which will provide such a base line, as well as contribute to an understanding of the alterations in charge density distributions associated with atomic ionization and excitation.

The study utilizes the "near Hartree–Fock quality" LCAO–SCF wave functions by Clementi, Roothaan, and Yoshimine (CRY functions), for the first row ground and excited states, and the Clementi functions for second row ground states and selected excited states and ground states of positive and negative ions.[4] For the basis set comparisons, the unpublished Bagus–Gilbert (BG) accurate functions are used.[5] While the CRY and Clementi functions originate from the same source and would appear to possess the same computational precision, it is not clear that they possess the same degree of accuracy when first row functions are compared to second row or neutral ground state configurations are compared to ionized or excited state configurations. What appears to be discrepancies in quality arose in the course of analysis; these are given brief description and discussion in the appropriate place.

Definitions

The following numerical parameters, derived from the atomic electron charge density, are defined for the purposes of this paper.

The total electron charge density at the nucleus, ρ_N, is called the *nuclear electron density*, or *electron density at the nucleus*, which may be computed for any free or bound atom.

Integration of the spherical electron charge density over a specified volume yields a number called the electron population, $P(n)$, which may assume any value (fractional or integral) up to N, the number of elec-

(1) (a) Harvard Medical Unit, Boston City Hospital; (b) Department of Physics, University of Louisville.

(2) (a) R. F. W. Bader, W. H. Henneker, and P. E. Cade, *J. Chem. Phys.*, 46, 3341 (1967); (b) R. F. W. Bader, I. Keaveny, and P. E. Cade, *ibid.*, 47, 3381 (1967); (c) R. F. W. Bader and A. D. Bandrauk, *ibid.*, 49, 1653 (1968); (d) P. E. Cade, R. F. W. Bader, W. H. Henneker, and I. Keaveny, *ibid.*, 50, 5315 (1969); (e) P. E. Cade, R. F. W. Bader, and J. Pelletier, *ibid.*, 54, 3517 (1971).

(3) (a) T. Berlin, *ibid.*, 19, 208 (1951); (b) B. J. Ransil and J. J. Sinai, *ibid.*, 46, 4050 (1967).

(4) E. Clementi, C. C. J. Roothaan, and M. Yoshimine, *Phys. Rev.*, 127, 1618 (1962); E. Clementi, *IBM J. Res. Develop., Suppl.*, 9, 2 (1965).

(5) P. Bagus and T. Gilbert, private communication.

Table I. Calculated Nuclear Electron Densities for Ground State First and Second Row Atoms (e/bohr³)

Atom	Total energy, hartrees BG[a]	Total energy, hartrees CRY[b]	Nuclear electron density, ρ_N, e/bohr³ BG	Nuclear electron density, ρ_N, e/bohr³ CRY	Basis set composition —BG STO's— 1s	2s	3s	p	—CRY STO's— 1s	2s	3s	p
He	−2.861680	−2.861680	3.60087	3.59613	1	2			5			
Li	−7.432726	−7.432726	13.8347	13.8350	2	3			2	4		
Be	−14.57302	−14.57302	35.4196	35.4301	2	2	1		2	4		
B	−24.52906	−24.52905	71.9861	71.9330	2	2	1	4	2	4		4
C	−37.68862	−37.68861	127.575	127.504	2	2	1	4	2	4		4
N	−54.40093	−54.40091	206.096	205.953	2	2	1	4	2	4		4
O	−74.80938	−74.80936	311.908	311.816	2	2	1	4	2	4		4
F	−99.40933	−99.40928	448.736	448.514	2	2	1	4	2	4		4
Ne	−128.5471	−128.5470	620.354	619.749	2	2	1	4	2	4		4
Na	−161.8585	−161.8589	833.515	833.234	2	1	3	3	1		7	5
Mg	−199.6143	−199.6146	1093.40	1093.07	1	2	3	3	1		7	5
Al	−241.8765	−241.8767	1402.06	1402.04	1	2	3	5	1		7	8
Si	−288.8542	−288.8543	1764.54	1764.54	1	2	3	5	1		7	8
P	−340.7186	−340.7189	2185.14	2185.32	1	2	3	5	1		7	8
S	−397.5046	−397.5048	2666.82	2668.31	1	2	3	5	1		7	8
Cl	−459.4816	−459.4819	3215.05	3218.31	1	2	3	5	1		7	8
Ar		−526.8173		3837.96					1		7	8

[a] P. Bagus and T. Gilbert, private communication. [b] See ref 4.

trons in the atom, depending on the volume over which the integration is performed. For atoms we define *integer electron populations*, $P(1)$, $P(2)$, etc., obtained by integrating the spherical atom density over a volume just sufficient to yield an integer electron population of 1, 2, 3, etc. $P(e)$ refers to any integer electron population. The *atomic core* P_K P_L, etc., and *closed shell populations* $P(1s^2) = P(2)$, $P(1s^2\ 2s^2) = P(4)$, and so on, are special cases of $P(e)$.

Each of these populations is associated with radii, called *integer electron radii*, $r(1)$, $r(2)$, $r(e)$, that define a sphere enclosing sufficient density to yield the respective integer electron population upon integration.

These parameters may be used, in ways that will be demonstrated, to give precise measures of spatial shifts in charge density distribution associated with atomic excitation and ionization and to compare the "equivalence" and "accuracy" of wave functions. Their relevance to molecule formation will be treated elsewhere.

Wave Function Comparisons. Quality of LCAO–SCF Wave Functions

By Comparison of Nuclear Electron Densities. Two wave functions with equivalent total energy may have demonstrably different charge density properties. For example, comparing the nuclear charge density, ρ_N, associated with two sets of energetically comparable atomic functions, CRY and BG-accurate, for which the total energies are equal to six significant figures, Table I shows that in many cases the nuclear charge densities differ in the fourth significant figure.

Inspection of the respective basis set compositions suggests that the observed differences in ρ_N arise primarily from the differences in the number and kinds of s functions. The CRY functions use six s-type functions (two 1s and four 2s STO's) and the BG functions use five (two 1s, two 2s, and one 3s STO's). The same number of 2p functions is used in both basis sets but neither the 2p orbital exponents nor AO coefficients (not shown) are as similar as the agreement in total energy would lead one to expect, which suggests that the orbital exponents and AO coefficients for the p functions are affected by the number and type of s functions utilized in the basis set.

Because they possess a node at the origin, the 2s and 2p STO's do not contribute *directly* to ρ_N, which suggests that the difference in ρ_N between the two sets might be attributed to the dissimilarities in 1s function representation. However, both the 2s and 2p STO's contribute *indirectly* to ρ_N through the nonorthogonality relationship of the 1s–2s STO's and the fact that the angle-averaged 2p STO reduces to a 2s STO.

The individual STO product contributions to ρ_N arising from different basis set representations can be considerably different, producing the differences noted in Table I. The dissimilarities in density between two different functions are not necessarily confined to the nucleus but may occur anywhere in density space. Precise measures for these differences are provided by density difference diagrams and integer electron radii, discussed in the next sections. On the basis of the observed differences in nuclear electron densities, these wave functions may therefore be judged "nonequivalent" though energetically equal.

The experimental analog of the electron density at the nucleus, Q_0^e, appears as a factor in the theoretical expression for isomer shift measurements. Such measurements are made on bulk samples, from which shifts in electron density at the nucleus (relative to some reference substance) can be determined if the radial shifts are known.[6] The computation of close-to-accurate Hartree–Fock wave functions for suitable solid state aggregates such as the unit cell is now within grasp. While it is not possible to obtain the electron density or density shifts at the nucleus by isomer shift measurements for free atoms (the systems treated in this paper), the potential for application to larger aggregate systems should be realized. In these cases a measure of wave function "accuracy," in addition to the energy estimate, would be agreement with experimental values of Q_0^e obtained from Mössbauer and Knight shift measurements.

(6) G. Wertheim, "Mössbauer Effect. Principle and Applications," Academic Press, New York, N. Y., 1963, pp 49–54.

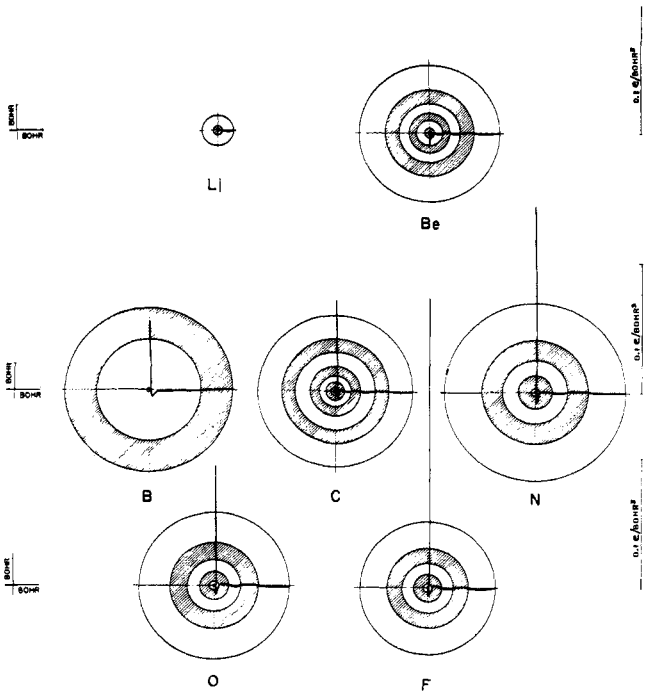

Figure 1. $\Delta\rho$(BG–CRY) maps and $\Delta\rho$(BG–CRY) profiles for first row atoms. Cross-hatched areas indicate charge buildup of the BG function relative to the CRY function. The left-hand scales refer to the $\Delta\rho$ maps and the right-hand scales to the $\Delta\rho$ profiles.

By Charge Density Differences. Another way to compare the two energetically equivalent wave functions is by analyzing their charge density difference ($\Delta\rho$) maps as in Figure 1. Superimposed on the difference maps are difference profiles. The $\Delta\rho$ maps show how the respective atomic density distribution functions differ in atom space, while the superimposed $\Delta\rho$ profiles show the relative magnitudes of the difference.

In general the greatest density differences occur at the nucleus and at radial distances out to approximately 0.5–0.75 bohr. Beyond that the density differences are of the order 10^{-4} density unit. The 0.5–0.75 bohr, for which distinctly different distribution patterns are found, represents about one-third of the total charge. The less striking density differences over the rest of atom space involve the remaining two-thirds of the charge.

When plotted against atomic number, the quantity $\Delta\rho_N$(BG–CRY) is too high for the N atom and too low for the O atom. The same seems true as well for the second row $\Delta\rho_N$(BG–CRY) values, where Al seems a bit too low and P a bit too high, compared to the rest of the series. Log–log plots of 1s orbital exponents as a function of atomic number show minor fluctuations about the straight line of the rest of the series, suggesting that the above discrepancies may arise from incomplete s-orbital optimization.

The existence of significant density differences between two free atom functions of equal total energy but different STO composition will yield noticeably different molecular $\Delta\rho$ maps constructed from the different functions. As an example of this consider the atomic $\Delta\rho$(BG–CRY) map for F in Figure 1. At 1.34 bohrs (one-half R_e for F_2) the map shows that the BG atom density is greater than the Clementi atom density. Consequently for F_2, all else being equal, one would expect to find a greater buildup of charge at a radial distance $r = 1.34$ bohrs from each nucleus in the molecular $\Delta\rho$ map constructed from Clementi functions.

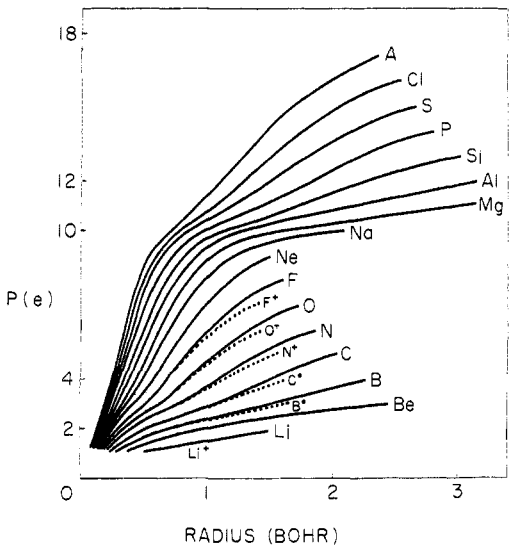

Figure 2. Integer electron populations as a function of atomic radius for ground state first and second row atoms and first row positive ions.

These expectations are confirmed when the two different molecular $\Delta\rho$ maps are compared, using Figure 3 from Bader, Henneker, and Cade (ref 2a, constructed from Clementi atom functions) and Figure 9, Case B, RS 1967 (using BG atom functions).

While molecular $\Delta\rho$ populations ($\Delta\rho$ integrated over an appropriate $\Delta\rho$ region) in the example cited differ significantly, it is not yet certain that the differences are large enough to affect materially either the total ρ population (total ρ integrated over the $\Delta\rho$ region in question) in the same region or the interpretation of bond formation in terms of localized electron populations. While these matters are the domain of molecular analysis, their dependence upon the differences that arise in atomic charge distributions should be kept in mind.

By Integer Electron Radii. A third method for comparing energetically equivalent wave functions utilizes the integer electron radii as provided in Table II for first and second row ground states. To assist the reader in visualizing these radii, Figure 2 shows the integer electron populations P(e) as a function of their associated radii for first and second row neutral atoms and first row positive ions. The smoothness of the curves provide a check of calculational consistency.

The significance of the curves is best conveyed by an example. Taking neon and correlating slope changes with P(e) values, it is noted that for $P(e) \leq 2$ ($1s^2$ shell), the curve rises abruptly with approximately constant slope. Thereafter $P(2) \rightarrow P(3)$ shows a decrease in slope; $P(3) \rightarrow P(4)$, an increase in slope; $P(4) \rightarrow P(7)$ (approximately) a further slight increase in slope; $P(7) \rightarrow P(10)$, an asymptotic leveling off, with a corresponding slope decrease, as P(e) approaches 10. (Asymptotic behavior not sketched.)

For argon, $P(e) \leq P(2)$ shows an abrupt rise with constant slope; $P(2) \rightarrow P(3)$, a slight but perceptible decrease in slope; $P(3) \rightarrow P(4)$, an increase in slope; $P(4) \rightarrow P(7)$ a further increase in slope; $P(7) \rightarrow P(10)$,

Table II. Integer Electron Radii for Ground State First and Second Row Atoms (bohrs)

P(e)	He	Li	Be	B	C	N	O	F	Ne
1	0.8090	0.5004	0.3591	0.2808	0.2305	0.1954	0.1694	0.1495	0.1337
2		1.5322	0.9851	0.7020	0.5371	0.4319	0.3603	0.3078	0.2678
3			2.4560	1.5297	1.0745	0.8105	0.6465	0.5303	0.4463
4				2.2944	1.5035	1.1000	0.8622	0.6998	0.5835
5					2.0729	1.4163	1.0793	0.8610	0.7094
6						1.8779	1.3430	1.0400	0.8418
7							1.7486	1.2679	0.9957
8								1.6287	1.1969
9									1.5210
		Na	Mg	Al	Si	P	S	Cl	A
1		0.1206	0.1098	0.1007	0.0930	0.0864	0.0806	0.0756	0.0711
2		0.2368	0.2122	0.1921	0.1754	0.1613	0.1492	0.1388	0.1297
3		0.3855	0.3394	0.3029	0.2734	0.2487	0.2281	0.2105	0.1952
4		0.5011	0.4391	0.3909	0.3512	0.3188	0.2916	0.2685	0.2486
5		0.6063	0.5293	0.4693	0.4212	0.3818	0.3487	0.3206	0.2965
6		0.7155	0.6221	0.5500	0.4925	0.4455	0.4063	0.3732	0.3447
7		0.8405	0.7275	0.6410	0.5724	0.5166	0.4704	0.4314	0.3979
8		1.0010	0.8614	0.7556	0.6725	0.6051	0.5497	0.5030	0.4631
9		1.2533	1.0679	0.9296	0.8224	0.7360	0.6654	0.6063	0.5561
10		2.1272	1.6286	1.3538	1.1564	1.0072	0.8911	0.7976	0.7208
11			3.0406	2.2100	1.7403	1.4359	1.2249	1.0663	0.9430
12				3.1815	2.2968	1.8178	1.5152	1.2969	1.1321
13					3.0414	2.2359	1.8070	1.5169	1.3066
14						2.8426	2.1578	1.7584	1.4879
15							2.6931	2.0622	1.6957
16								2.5385	1.9637
17									2.3899

Table III. Effect of Basis Set Expansion on Integer Electron Radii and Electron Density at the Nucleus for the Be Atom

Function	Total energy, hartrees	ρ_N, e/bohr^3	First electron $r(1) = 0.3591$ bohr[a]	Second electron $r(2) = 0.9851$ bohr[a]	Third electron $r(3) = 2.4560$ bohrs[a]	Basis set composition
BG minimal[b]	−14.55674	33.0334	1.0111	2.0131	2.9731	1s, 2s
BG marginal	−14.57209	35.2610	1.0006	2.0006	2.9938	1s, two 2s
BF nominal	−14.57299	35.4057	1.0000	2.0001	3.0005	two 1s, 2s, 3s
BG accurate	−14.57302	35.4196	1.0000	1.9999	2.9998	two 1s, two 2s, 3s
CRY[c]	−14.57300	35.4301	1.0000	2.0000	3.0000	two 1s, four 2s
Experimental	−14.6699					

[a] From Table II. [b] See ref 5. [c] See ref 4.

a marked change in curvature with marked decrease in slope; $P(10) \rightarrow P(11)$, a further slight but perceptible decrease in slope; $P(11) \rightarrow P(12)$, a slight increase in slope; $P(12) \rightarrow P(15)$, a further slight increase in slope; $P(15) \rightarrow P(18)$, a marked change of curvature with marked slope decrease, as the curve asymptotically approaches $P(18)$.

If a slope increase and decrease implies a decrease and increase in radius per unit charge addition respectively, the diagram succinctly shows the charge cloud contraction and expansion associated with the successive addition of electrons by the aufbau principle and the relative changes in radius associated with each shell or subshell.

Figure 2 further demonstrates the increase in radius with increase of effective nuclear charge for each isoelectronic series. Plots of radius as a function of Z for each isoelectronic series can also be obtained from Table II. Finally, a radius increase for valence electrons (but not inner shell electrons) associated with positive ion formation is clearly shown.

An example of how charge density data may be used to compare atom functions of differing quality is provided by Table III for the Be atom. In the K-shell region, defined by the integer electron radii, $r(1) = 0.3591$ bohr and $r(2) = 0.9851$ bohr, the electron population $P(e)$ for the various BG functions *increases* as the approximation *decreases* in quality, if the latter is judged on the basis of total energy. In this region the inferior approximations appear to *overestimate* the number of electrons per unit volume. The converse is true for the first L-shell electron, $2s^1$. At its BG–accurate 3-electron radius $r(3) = 2.4560$ bohrs, the BG–minimal population is 2.9731 e, not 3 e, the difference, 0.0269 e, providing a quantitative measure of the difference in electron charge predicted by the two comparable functions for this specific region of space.

Further, examination of the ρ_N data in Table III shows that ρ_N decreases as the approximation decreases in accuracy (on the basis of total energy), which suggests that further expansion of basis set by addition of s-type STO's (because these are the principle contributors to ρ_N) should decrease the total energy and increase ρ_N.

Comparison of the BG–accurate and CRY basis sets with their respective nuclear electron densities strongly suggests that a saturation point might exist such that no further increase in ρ_N occurs with further addition and optimization of the appropriate s-type STO's. Because both functions are energetically equivalent,

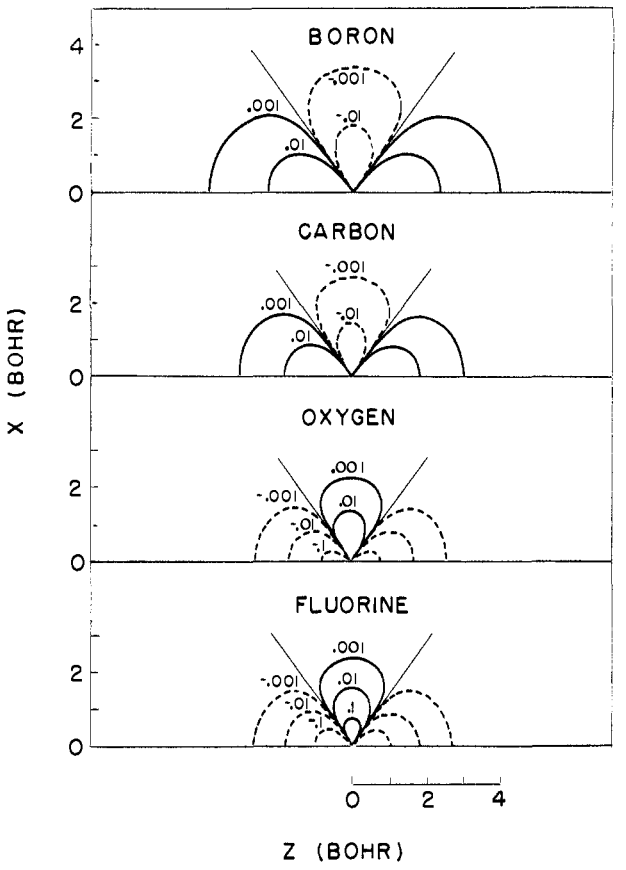

Figure 3. $\Delta\rho$(valence-averaged) maps for boron, carbon, oxygen and fluorine atoms.

maximization of ρ_N, or where applicable, agreement with the experimental quantity Q_0^e, might very well provide a second criterion, in addition to energy minimization, by which wave function accuracy may be judged or at least by which expansion to the Hartree–Fock limit may be achieved with greater rapidity and confidence. But this possibility must be considered strictly speculative at this time.

From the data of Table III it would appear that the two best wave functions for Be, CRY and BG-accurate, are very nearly identical because their total energies and core populations are very nearly equal within the limits of calculational precision. On the other hand, the ρ_N values differ in the fourth significant figure by 0.03% which, while not large, is nevertheless a real discrepancy arising from the differences in the composition of the basis set, *i.e.*, two 1s, two 2s *vs.* two 1s, four 2s STO's.

This discrepancy could prove to be a significant source of error for the calculation of properties dependent on electron charge density at or close to the nucleus, for example, dipole moments and the core electron contributions to X-ray scattering factors and Compton profiles. With respect to the latter the fact that the locus of each electron (as estimated by the integer electron radius) can change, depending on the basis set representation, introduces a degree of ambiguity which is usually construed as "disagreement between theory and experiment," when it could as well represent inadequate s-type saturation and/or inadequate optimization.

Further, the assumption that the atomic "core" from which the electron or X-ray beams are deflected in a solid is the core defined by the free atom K and L shell populations, should be regarded as a convenient first approximation which may be expected to hold reasonably well only where the free atom and the bound atom densities are very similar over a reasonably large intramolecular volume, such as Li compounds.

Averaged and Valence Distributions

Because molecular $\Delta\rho$ maps are constructed as a difference between the molecular density distribution and the distributions of its dissociation products, the density difference patterns obtained depend upon the assumptions made concerning the electron configurations of the dissociation products. Considerably different molecular $\Delta\rho$ maps will result depending on whether the end products are neutral or ionic species, in ground or excited states.

Further, where the dissociation products are free atoms or ions, the density distributions may be averaged over angle, or one may choose a valence state appropriate to the chemical situation. While the angle-averaged distribution is spherical, the valence density distribution for atoms with partially filled orbitals possessing nonzero angular momentum possesses a characteristic symmetry. Significant differences between the two mappings occur in those atoms possessing partially occupied p orbitals (B, C, O, and F atoms) which, in the case of the valence distributions, have been filled according to the convention adopted by Bader, *et al.*: one electron in the p_σ orbital, the remainder averaged over the p_π orbitals.[7]

One illuminating way of visualizing the effect the valence distributions will have on the molecular $\Delta\rho$ map, compared to the averaged distribution, is by mapping the density difference between the atomic valence and averaged distributions, $\Delta\rho$(valence-averaged). Figure 3 presents such maps for B, C, O, and F atoms. The maps show a charge buildup along the bond axis for the valence configurations of B and C relative to their averaged distributions but a charge deficit along the bond axis for the valence configuration of O and F. In other words the valence distribution contributes greater charge density to the overlap regions for B and C than does the spherically averaged distribution, but less in the case of O and F. The actual number of electrons involved can be determined by an appropriate integration.

The $\Delta\rho$(valence-averaged) maps for the CRY and BG first row atom functions were found to be identical numerically despite different orbital exponent values. This is presumably because they represent the density difference arising solely from the angle-averaging effect and the number of 2p STO's, and hence the angular dependency, is the same for both sets.

Given these differences between the valence and averaged charge density distributions, what are the principal features to be expected from any diatomic molecular $\Delta\rho$ map constructed with averaged or valence atomic distributions? The averaged distributions produce a *greater charge buildup* in the internuclear regions for B and C, relative to the dissociated atoms, than do the valence distributions, while the reverse is true for O and F.

(7) See ref 2a, p 3345; and ref 2b, p 3386.

Table IV. Integer Electron Radii (bohr) and Electron Densities at the Nucleus (e/bohr^3) for First and Second Row Excited Atoms

	Carbon			Nitrogen			Oxygen		
P(e)	^{3}p	^{1}d	^{1}s	^{4}s	^{2}d	^{2}p	^{3}p	^{1}d	^{1}s
1	0.2304	0.2304	0.2304	0.1954	0.1954	0.1953	0.1694	0.1694	0.1694
2	0.5371	0.5386	0.5405	0.4319	0.4328	0.4335	0.3603	0.3607	0.3612
3	1.0745	1.0813	1.0912	0.8105	0.8152	0.8184	0.6456	0.6472	0.6498
4	1.5035	1.5170	1.5375	1.1000	1.1084	1.1141	0.8622	0.8650	0.8692
5	2.0729	2.1026	2.1513	1.4163	1.4312	1.4414	1.0793	1.0839	1.0906
6				1.8779	1.0968	1.9272	1.3430	1.3506	1.3621
7							1.7486	1.7628	1.7854
ρ_N	127.504	127.486	127.620	205.953	206.120	206.242	311.816	311.894	311.948
Energy, hartrees	−37.68861	−37.63131	−37.54954	−54.40091	−54.29615	−54.22809	−74.80936	−74.72921	−74.61095
	Silicon			Phosphorus			Sulfur		
1	0.0930	0.0930	0.0930	0.0864	0.0864	0.0864	0.0806	0.0806	0.0806
2	0.1754	0.1754	0.1754	0.1613	0.1614	0.1614	0.1492	0.1493	0.1493
3	0.2734	0.2733	0.2733	0.2487	0.2488	0.2488	0.2281	0.2281	0.2281
4	0.3512	0.3512	0.3512	0.3188	0.3188	0.3188	0.2916	0.2916	0.2917
5	0.4212	0.4212	0.4212	0.3818	0.3817	0.3818	0.3487	0.3487	0.3487
6	0.4925	0.4926	0.4925	0.4455	0.4455	0.4456	0.4063	0.4064	0.4064
7	0.5724	0.5725	0.5725	0.5166	0.5167	0.5168	0.4704	0.4705	0.4705
8	0.6725	0.6725	0.6725	0.6051	0.6053	0.6054	0.5497	0.5498	0.5499
9	0.8224	0.8226	0.8227	0.7360	0.7363	0.7364	0.6654	0.6656	0.6658
10	1.1564	1.1572	1.1578	1.0072	1.0079	1.0083	0.8911	0.8916	0.8919
11	1.7403	1.7455	1.7516	1.4359	1.4395	1.4417	1.2249	1.2266	1.2281
12	2.2968	2.3114	2.3314	1.8178	1.8265	1.8325	1.5152	1.5185	1.5225
13	3.0414	3.0814	3.1436	2.2359	2.2541	2.2665	1.8070	1.8128	1.8206
14				2.8426	2.8828	2.9100	2.1578	2.1683	2.1827
15							2.6931	2.7146	2.7436
ρ_N	1764.54	1764.95	1765.37	2185.32	2185.40	2185.62	2668.31	2668.42	2668.60
Energy, hartrees	−288.8543	−288.8150	−288.7584	−340.7187	−340.6487	−340.6032	−397.5046	−397.4521	−397.3744

If, as believed but unproved, a positive $\Delta\rho$ correlates with some measure of chemical bonding or binding, the averaged distributions are compatible with a stronger σ bond in B and C but a weaker σ bond in O and F, compared to the valence distributions, because the σ-oriented $\Delta\rho$ regions are larger and smaller, respectively.

On the other hand, the π-oriented $\Delta\rho$ regions in a diatomic molecule appear as distinct, nonoverlapping accumulations of charge focused on each atom, representing regions of greater electron charge buildup in the molecule, relative to free-atom superposition. The greater the charge buildup in the vicinity of each center, the greater the electron repulsion between centers, such that an increased charge buildup in the π direction on each atom seems consistent with weakening of the π bond. Viewed in this manner the averaged distributions correlate with stronger π bonding in B and C than the valence distributions and weaker π bonding in O and F. These findings are consistent with the general characteristics of B, C, O, and F chemistry, which supports the use of averaged charge distributions. The difficulty with this analysis, apart from its lack of quantitative verification, is that for the time being one assumes what must be demonstrated for molecular bond formation; that is, a positive $\Delta\rho$ as defined here relates in some manner to chemical binding or bonding.

For the atoms considered, both wave functions are energetically equivalent and the sets of p orbitals from which each were constructed are equivalent representations. Hence, from the standpoint of total energy, neither electron distribution can be preferred over the other. Because the distributions are energetically equal and because molecule formation implies presence of a field which in turn implies certain preferred p-orbital fillings, Bader *et al.*, compute their molecular $\Delta\rho$ diagrams from the atomic ground state valence distributions as the construction that provides the "maximum amount of chemical information." [8]

At this point in development, neither approach may be ruled in or out conclusively until the validity of the theory using both constructs has been established or rejected, presumably by relating the molecular $\Delta\rho$ maps to chemical binding.[9] It is sufficient to point out here that the differences existing between averaged and valence distributions may be quantitatively compared by the density diagrams and parameters and their relative effects on the molecular $\Delta\rho$ map predicted.

Charge Density Redistribution Associated with Atomic Excitation

While useful in evaluating wave function equivalence and accuracy, the principle value of charge density analysis is the information that may be inferred about structural problems. For atoms an appropriate application is the alteration of electron charge distribution associated with excitation and ionization. Table IV and Figure 4 supply the charge density data relevant to excitation arising from redistribution of p electrons among higher energy p levels.

Table IV reveals a consistent trend between the total energy and ρ_N for all cases but carbon. With

(8) See ref 2a.

(9) See RS 1967 for a more detailed discussion of this problem. Conclusions similar to these were again recently published by D. B. Boyd, *J. Chem. Phys.*, **52**, 4852 (1970).

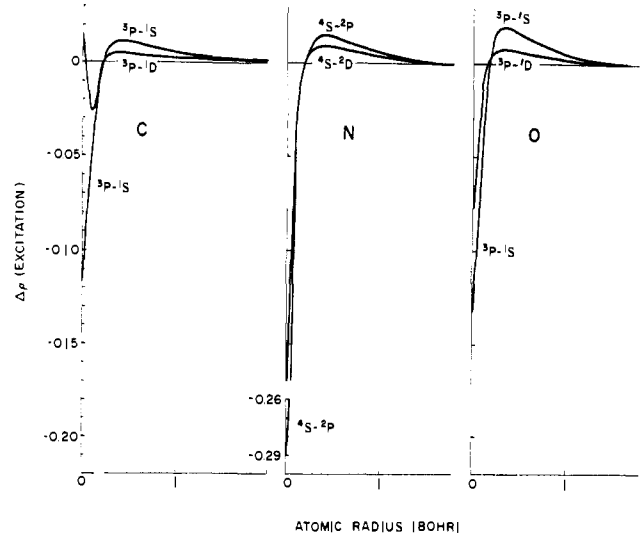

Figure 4. $\Delta\rho$(excitation) profiles for carbon, nitrogen, and oxygen.

that exception, the smallest ρ_N corresponds to the ground state. For states of equal multiplicities but different angular momentum, the smaller ρ_N corresponds to the state with the larger total angular momentum. The exception found in carbon may be real or it may be the result of internal inconsistencies in the neutral and/or excited state wave functions, similar to those cited earlier for the neutral O and N atoms. Suitable plots of individual orbital exponents against atomic number again suggest that the wave functions are not internally consistent.

Examining the integer electron radii for first row (2p electron) excitation (Table IV), only the $1s^1$ charge density radius, $r(1)$, remains unchanged, while the larger radii are noticeably increased. For 3p excitation (Si, P, and S atoms), $r(1) \rightarrow r(7)$ (*i.e.*, the radii corresponding to $1s^2$, $2s^2$, and $2p^3$ electrons) remain unchanged. The outer 2p radii, $r(8) \rightarrow r(10)$, increase slightly, while the larger radii, corresponding to the 3s and 3p electrons, increase markedly.

It would appear that with the exception of the C atom, atomic excitation arising from rearrangement of the 2p electrons for the first row atoms studied involves the following charge density distribution alterations: (1) an increase in ρ_N, (2) no change in $r(1)$, and (3) decrease in density of the outer electron distribution. Second row excitation by rearrangement of the 3p electrons entails (1) an increase in ρ_N, (2) no alteration of $r(1) \rightarrow r(7)$, and (3) a decrease in density of the outer electron distribution.

Figure 4 places the crossover between increased and decreased density, relative to the ground state, at about $r = 0.25$ bohr. The quantity of charge represented by both areas is equivalent.

The primary structural change associated with excitation of the 2p electrons is seen to be a shift of charge to the nucleus, at the expense of the outer lying regions. This is done in such a way that the radial intercepts of certain integral electron distributions remain fixed. Constancy of these radii implies only that within the unit-charge sphere defined by them, there has been no overall loss or gain of charge; the actual radial distribution in these regions may alter significantly, as Figure 4 shows. These constant radii define certain integral electron populations lying close to the nucleus that undergo no quantitative change during p-electron excitation compared to the ground state distribution, despite changes in both total energy and outer electron configuration of the atom.

Numerically the populations corresponding to these isodense distributions do not correspond to the classical K and L shell populations, $1s^2$ and $2s^2\ 2p^6$. Rather, in the first row, the integer electron radius remaining unchanged during excitation is that corresponding to the $1s^1$ electron distribution, while in the second row it is the integer electron radius corresponding to the electron distribution $1s^2\ 2s^2\ 2p^3$ that remains unchanged or fixed. The electron density distributions associated with the remaining electrons possess larger integral electron radii that reflect the decrease in density, relative to the ground state distribution, in these regions.

Figure 4 shows similar $\Delta\rho$(excitation) patterns for all but the C atom. As noted earlier, the electron density at the neutral C nucleus appears to be unaccountably large, producing the upturn in the $\Delta\rho(^3p-^1s)$ diagram observed at $r = 0.2$ bohr. Similarly, while the $\Delta\rho$ diagrams for the N excited states appear consistent with the O atom and one of the C atom curves, the $\Delta\rho_N(^4s-^2p)$ value seems excessively large. It is not known if this behavior is real or is attributable to the possibility that the CRY first row excited atom functions are not internally consistent with regard to basis set contributions to ρ_N. A detailed examination of these functions would seem in order.

To summarize, in all cases except $\Delta\rho(^3p-^1d)$ for the C atom, excitation by rearrangement of p-orbital filling results in an increase in electron density, relative to the neutral atom, at and near the nucleus, with a decrease in density over the rest of space. The approximate radial distance intersecting the regions of charge increase and decrease is $r = 0.25$ bohr.

Charge Density Redistribution Associated with Ionization

While the changes in density distribution for the excited atoms, relative to the ground state, arise from reassignment of p electrons to higher energy levels, the density distribution alterations occurring in single ion formation arise from the gain or loss of a p electron. The data of Table V show that for all first row atoms

Table V. Calculated Nuclear Electron Densities for Free Atom Single Ions (e/bohr^3)

Atom	Positive ion	Neutral atom	Negative ion
Li	13.6974	13.8350	13.8313
Be	35.2752	35.4301	
B	72.6381	71.9330	71.6794
C	128.522	127.504	126.968
N	207.418	205.953	205.489
O	313.291	311.816	311.095
F	450.356	448.514	447.360
Ne	622.304	619.749	
Na	833.441	833.234	834.056
Mg	1093.05	1093.07	
Al	1403.38	1402.04	1402.59
Si	1766.63	1764.54	1765.12
P	2187.58	2185.32	2185.49
S	2670.34	2668.31	2668.81
Cl	3219.99	3218.31	3218.56
Ar	3841.26	3837.96	

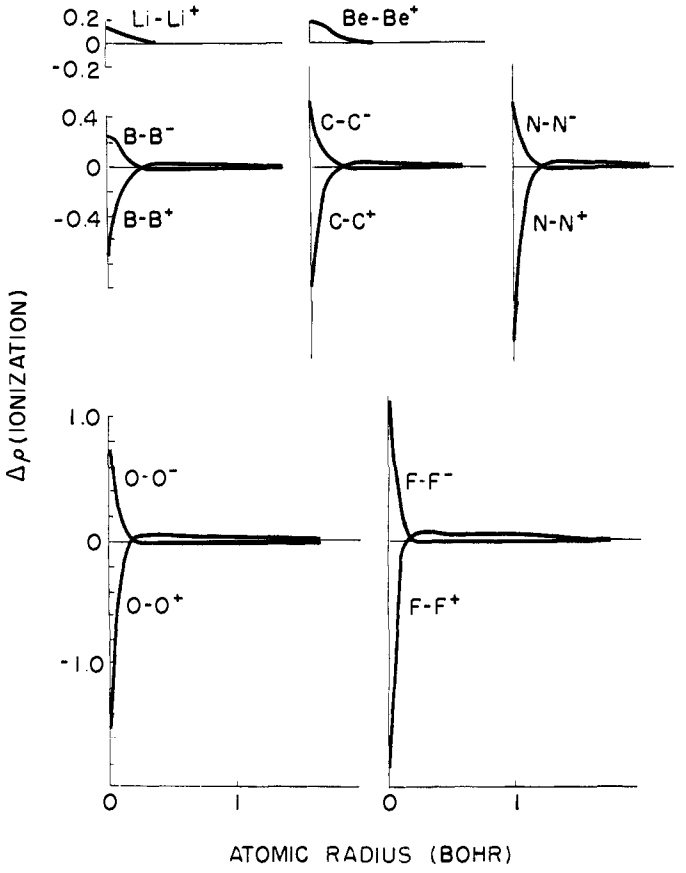

Figure 5. $\Delta\rho$(ionization) profiles for first row atoms.

except Li and Be electron addition (meaning $A^+ \rightarrow A \rightarrow A^-$) lowers the value of ρ_N. A different trend appears in the second row where both the positive and negative ion values of ρ_N are larger than the neutral atom ground states for most of the series.

Detailed comparisons of the wave functions indicate that the sets of wave functions, especially the second row negative ion functions, do not appear to be of comparable quality, particularly with regard to s function saturation and basis set contributions to computed ρ_N values. Rated in order, the quality of the functions would seem to be first and second row positive ions > first row neutral ~ second row neutral > first row negative ion > second row negative ion. Because the analysis and interpretation of ρ_N as a series depends on the use of accurate, comparable quality wave functions, it seems best to postpone extensive interpretation of the single-ion ρ_N data until the doubts along these lines raised by the analysis are resolved.

Turning to the $\Delta\rho$(ionization) maps for the first row atoms, Figure 5 illustrates the redistribution of electron density, relative to the neutral atom, $\Delta\rho(A\text{–}A^{\pm})$, associated with removal or addition of an electron, as a function of atomic (ionic) radius for first row atoms. $\Delta\rho$ profiles for Li–Li^- and Be–Be^- are not shown because $\Delta\rho$(Li–Li^-) is very small (about 10^{-4} density units) over the entire range and the wave function for Be^- is not available.

From the available data it appears that the formation of both Li and Be positive ions is associated with a decrease in electron charge density at and close to the nucleus, together with a density increase over the rest of atom space. In the case of Be^+ a narrow region of

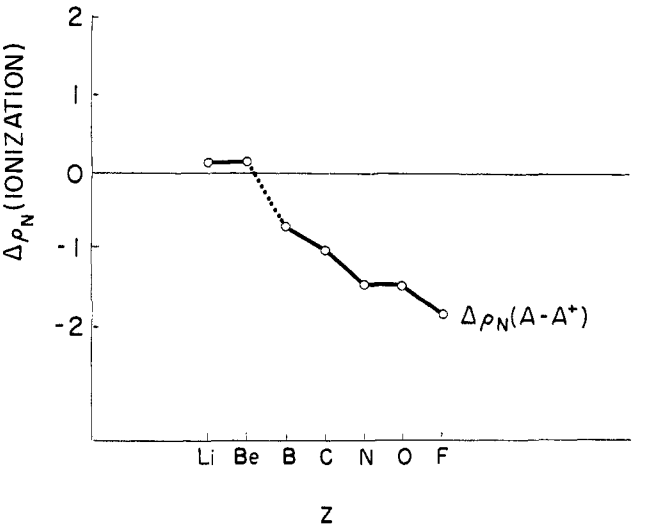

Figure 6. $\Delta\rho_N$(ionization) as a function of atomic number for first row positive ions.

charge buildup is found in the region $0.45 < r < 0.65$ bohr, followed by density depletion over the rest of space. Removal of the electron in both cases seems to affect the *inner* rather than the outer electron density distribution; that is, the greatest charge density depletion occurs at and very close to the nucleus which is usually viewed as the average locus of the K shell. In contrast, single positive ionization in these elements is usually visualized as removal of an L-shell electron.

The remaining positive ions in the first row series, $B^+ \rightarrow F^+$, show the reverse pattern. Removal of one p electron results in a charge buildup relative to the neutral atom at and close to the nucleus ($r < 0.3$ bohr), implying more nuclear screening together with a charge depletion over the rest of ion space. This pattern, it will be recalled, is similar to that found for p-electron excitation, which may be viewed as an early stage of p-electron removal. On the other hand, addition of an electron ($B^- \rightarrow F^-$) results in depletion of charge (reduced nuclear screening) relative to the neutral atom at and close to the nucleus ($r < 0.3$ bohr) and a buildup of charge over the rest of ion space. The number of electrons involved in the charge buildup or depletion may be determined from Figure 5 by the appropriate integration. Both patterns are consistent with the usual visualization of these atoms, *i.e.*, a positive and negative charge cloud, respectively.

Such data are relevant to ionic bond formation. In the case of a purely ionic diatomic bond, subtraction of the positive and negative ion densities from the molecular density should produce a close-to-zero $\Delta\rho$ distribution over all space. Nonzero $\Delta\rho$ distributions, on the other hand, are a measure of the bond's departure from pure ionic character, the degree of ionic character being related to the localized $\Delta\rho$ populations.

Comparing the $\Delta\rho$(ionization) maps as a consecutive series, it is seen that the behavior of the $\Delta\rho$ profile maps for Li^+ and Be^+ qualitatively resemble the $\Delta\rho$ profile maps for $B^- \rightarrow F^-$. In terms of these profiles, the first row elements appear to be subdivided into two subgroups, Li and Be on the one hand, B → F on the other. A plot of $\Delta\rho_N(A\text{–}A^+)$ *vs.* atomic number (Figure 6) clearly demonstrates a "discontinuity" in the positive ion nuclear electron density values.

Table VI. Integer Electron Radii (bohrs) for Single Ions and Neutral Atoms

	P(e)	1	2	3	4	5	6	7	8	9
Li	Pos	0.5038								
	Neut	0.5004	1.5322							
	Neg									
Be	Pos	0.3614	1.0239							
	Neut	0.3591	0.9851	2.4560						
	Neg									
B	Pos	0.2794	0.7325	1.6884						
	Neut	0.2808	0.7020	1.5297	2.2944					
	Neg	0.2815	0.7019	1.5254	2.2130	3.2615				
C	Pos	0.2296	0.5477	1.1281	1.6575					
	Neut	0.2305	0.5371	1.0745	1.5035	2.0729				
	Neg	0.2311	0.5370	1.0704	1.4787	1.9516	2.6970			
N	Pos	0.1948	0.4364	0.8346	0.1543	1.5648				
	Neut	0.1954	0.4319	0.8105	1.1000	1.4163	1.8779			
	Neg	0.1958	0.4331	0.8140	1.1001	1.4003	1.7832	2.4170		
O	Pos	0.1691	0.3617	0.6541	0.8805	1.1224	1.4662			
	Neut	0.1694	0.3603	0.6456	0.8622	1.0793	1.3430	1.7486		
	Neg	0.1697	0.3608	0.6463	0.8612	1.0713	1.3126	1.6335	2.1736	
F	Pos	0.1492	0.3087	0.5357	0.9105	0.8825	1.0869	1.3932		
	Neut	0.1495	0.3078	0.5303	0.6998	0.8610	1.0400	1.2679	1.6287	
	Neg	0.1497	0.3081	0.5302	0.6986	0.8562	1.0259	1.2291	1.5049	1.9744

These findings are consistent with what is known about the bond character and dipole moments of the hydride molecules formed from these atoms. Both in solid and gas phase the LiH bond is ionic, represented by Li^+H^-, while the OH and HF bonds, also ionic, exhibit the reversed polarities, $O-H^+$ and H^+F^-. The calculated and experimental dipole moments show the same trend which has been interpreted as a discontinuity in bond type.[10]

The rearrangement of electron charge as a function of electron addition may be inferred from the integer electron radii of Table VI. Granting the uncertainty of the accuracy of the data due to different quality wave functions, the following observations are worth making. First, the discontinuity noted earlier between Li → Be on the one hand and B → F on the other appears again in the behavior of the integer electron radius $r(1)$ with electron addition. Secondly, contrary to what was found for excited atom radii, none of the integer electron radii remain unchanged with respect to the neutral ground state atom gradii.

For the most part, the integer electron radii of Table VI appear to follow a trend with respect to the addition of an electron. B → F show first an increase in $r(1)$ and then a decrease in all the other radii (with a few showing a minimum that may reflect "nonequivalent" functions) as an electron is successively added. This roughly corresponds to a decrease in the charge density very close to the nucleus and an increase in density over the rest of space, which is consistent with the increase in charge density to be expected with electron addition. In other words, relative to the neutral atom radii, the single ion radii are consistent with the notion of positively and negatively charged spheres.

(10) See, for example, K. Fajans, *J. Chem. Phys.*, **40**, 1773 (1964); 41, 4005 (1964); 43, 2159 (1965); S. M. Blinder, *ibid.*, 41, 4004 (1964); and P. Cade and W. M. Huo, *ibid.*, 45, 1063 (1966).

Conclusion

Comparison of certain charge density parameters derived from energetically equivalent atomic wave functions establish the nonequivalence of these functions in terms of their charge density distributions. The analysis leads to suggesting a second criterion, maximization of nuclear electron density, or agreement with its experimental equivalent Q_0^e, where applicable, as a criterion for calculating accurate wave functions.

Analysis of atomic valence and spherically averaged distributions provides strong plausibility arguments for utilizing the latter in constructing molecular maps from neutral ground state atoms.

It is established that p-electron excitation results in a charge buildup at and near the nucleus with a corresponding charge depletion elsewhere, in such a way that certain integer electron radii remain constant.

The quantitative effects of ionization by removal or addition of a p electron upon the charge density distribution are established. Positive ionization for B → F, like p-electron excitation, results in charge buildup at and near the nucleus relative to the neutral atom and a charge depletion elsewhere. Negative ionization results in depletion of charge at and near the nucleus with a corresponding buildup elsewhere.

Charge density analysis of single electron ionization demonstrates the existence of a "discontinuity" between the series Li → Be and B → F that parallels the discontinuity recently reported for dipole moment data.

Throughout the analysis small inconsistencies in the data arise which appear to be associated with incomplete saturation of the ion and excited atom basis sets and/or incomplete optimization of the orbital exponents.